Microwave transmission through a metal capped array of holes in a metal sheet

Matthew P. Biginton,[1,*] Alastair P. Hibbins,[1] J. Roy Sambles,[1] and Ian J. Youngs[2]

[1]*School of Physics, University of Exeter, Exeter, EX4 4QL, UK*
[2]*Defence Science & Technology Laboratory, Salisbury, Wiltshire, SP4 OJQ, UK*
**m.p.biginton@ex.ac.uk*

Abstract: The microwave response of a square array of "metal capped" holes in a metal sheet is explored both experimentally and numerically. Above each circular aperture are concentrically placed metallic discs, separated by a fraction of the wavelength, with discs having radii larger than the apertures. The volume bound by the overlap supports a family of resonances that mediate transmission with the fundamental resonant mode being a factor of ~2.3 lower in frequency than the bare aperture resonance.

OCIS codes: (100).0100) Image processing; (110.0110) Imaging systems; (100.2980) Image enhancement; (100.6890) Three-dimensional image processing; (100.3175) Interferometric imaging; (110.6880) Three-dimensional image acquisition.

References and links

1. E. C. Ngai, and A. P. Smolski, "Electromagnetic properties of metal space frame radomes for use in satellite communications earth stations," Antennas and Propag. Society International Symposium, AP-S Digest, **3**, 1956–1959, (1993)
2. T. W. Ebbesen, H. J. Lezec, H. F. Ghaemi, T. Thio, and P. A. Wolff, "Extraordinary Optical Transmission through Sub-wavelength Hole Arrays," Nature **391**(6668), 667–669 (1998).
3. E. A. Parker, and S. M. A. Hamdy, "Rings as elements for frequency selective surfaces," Electron. Lett. **17**(17), 612–614 (1981).
4. E. A. Parker, S. M. A. Hamdy, and R. J. Langley, "Arrays of concentric rings as frequency selective surfaces," Electron. Lett. **17**(23), 880–881 (1981).
5. E. A. Parker, and A. N. A. El Sheikh, "Convolted dipole array elements," Electron. Lett. **27**(4), 322–323 (1991).
6. R. Mittra, R. Hall, and C.-H. Tsao, "Spectral-domain analysis of circular patch frequency selective surfaces," IEEE Trans. Antenn. Propag. **32**(5), 533–536 (1984).
7. D. S. Lockyer, J. C. Vardaxoglou, and R. A. Simpkin, "Complementary frequency selective surfaces," IEEE Trans. Antenn. Propag. **147**(6), 501–507 (2000).
8. M. Beruete, R. Marques, J. D. Baena, and M. Sorolla, "Resonace and cross polarisation effects in conventional and complementary split ring resonantors periodic screens" Antenna and Propag. Society International Symposium., **3A**, 794–797, (2005)
9. I. Tardy, C. H. Chan, and J. S. Yee, "Analysis of the Yee Frequency Selective Surface" Antenna and Prop. Society International Symposium, AP-S Digest, **1**, 196–199, (1991)
10. A. P. Feresidis, G. Apostolopoulos, N. Serfas, and J. C. Vardaxoglou, "Closely coupled metallodielectric electromagnetic band-gap structures formed by double-layer dipole and tripole arrays," IEEE Trans. Antenn. Propag. **52**(5), 1149–1158 (2004).
11. D. S. Lockyer, C. Moore, R. Seager, R. Simpkin, and J. C. Vardaxoglou, "Coupled dipole arrays as reconfigurable frequency selective surfaces," Electron. Lett. **30**(16), 1258–1259 (1994).
12. is J. C. Vardaxoglou, and D. Lockyer, "Modified FSS response from two sided and closely coupled arrays," Electron. Lett. **30**(22), 1818–1819 (1994).
13. R. Pous, and D. M. Pozar, "A frequency selective surface using aperture coupled microstrip patches," IEEE Trans. Antenn. Propag. **39**(12), 1763–1769 (1991).
14. J. Shaker, and L. Shafai, "Removing the angular sensitivity of frequency selective surface structures using novel double-layer structures," IEEE Microw. Guid. Wave Lett. **5**(10), 324–325 (1995).
15. A. P. Hibbins, J. R. Sambles, C. R. Lawrence, and J. R. Brown, "Squeezing millimeter waves into microns," Phys. Rev. Lett. **92**(14), 143904 (2004).
16. N. Behdad, "A second-order band-pass frequency selective surface using non resonant sub wavelength periodic structures," Microw. Opt. Technol. Lett. **50**(6), 1639–1643 (2008).
17. M. J. Lockyear, A. P. Hibbins, J. R. Sambles, P. A. Hobson, and C. R. Lawrence, "Thin resonant structures for angle and polarisation independent microwave absorption," J. Appl. Phys. **94**, 041913 (2000).

#132940 - $15.00 USD Received 4 Aug 2010; revised 1 Oct 2010; accepted 3 Oct 2010; published 29 Oct 2010

18. B. A. Munk, *Frequency Selective Surfaces Theory and Design*, (John Wiley & Sons 2000)
19. Nelco, California, USA.
20. HFSS, Ansoft Corporation, Pittsburgh, PA, USA.

1. Introduction

Frequency selective surfaces (FSS) are essentially electromagnetic (EM) filters, and are used in a plethora of devices ranging from solar cells in the visible regime to applications of radar technology. The latter includes, for example, radomes, designed to protect a radar emitter/receiver from the wind, rain and sand while allowing the transmission of selected EM frequencies [1]. Ebbesen et al.'s work on holey metal films at optical frequencies [2] showed enhanced transmission close to the onset of diffraction with the resonant frequency dictated by the geometry of the hole. In the microwave regime many relatively simple arrays of metallic elements in a single layered FSS have been well-studied, including arrays of rings and dipoles [3–5], circular patches [6] and their complementary counterparts [7–9]. Several dual layered FSS [10–17], which offer a decreased sensitivity to changes in both polarization and angle of incidence, have also been explored.

Ebbesen et al's holey metal films transmitted more light than geometrically predicted. In this present work the holes (circular apertures) are capped with an array of circular metallic patches. In doing this the geometric gap through which light can pass at normal incidence is minimized. We investigate the electromagnetic interaction between the metal surfaces, and the resultant resonant transmission response. The capped aperture array is effectively composed of two closely spaced FSS layers, one of which is an array of copper circular patches while the other is a similar array of circular apertures in a copper sheet (Fig. 1). Each layer in isolation acts in the familiar FSS manner; the former exhibiting high pass behaviour (capacitive mesh) the latter demonstrates a low pass response (inductive mesh) [18]. The capped aperture array, is arranged so that the centre of each patch is directly above the centre of each aperture being spaced from one another by a low loss dielectric. The radius of the patches (r_1) exceeds the radius of the apertures (r_2) thereby creating an annular-shaped overlap region. This overlap region supports a family of resonant modes that mediate resonant transmission. By analogy to the modes supported by an annular waveguide (i.e., coaxial waveguide), one can approximate the resonant frequencies of the annular cavity to be

$$f_m = \frac{mc}{2\pi r_m n} \tag{1}$$

Here f_m is the frequency of the m^{th} resonance, $r_m = (r_1 + r_2)/2$ is the mean radius of the overlap volume, c is the speed of light in free space and n is the refractive index of the dielectric spacer. Equation (1) assumes that there is no penetration of the electric fields into the metal and no fringing at the edges of the overlap cavity, *i.e.*, in the limit that the spacing between the two FSS (t_d) tends to zero.

#132940 - $15.00 USD Received 4 Aug 2010; revised 1 Oct 2010; accepted 3 Oct 2010; published 29 Oct 2010

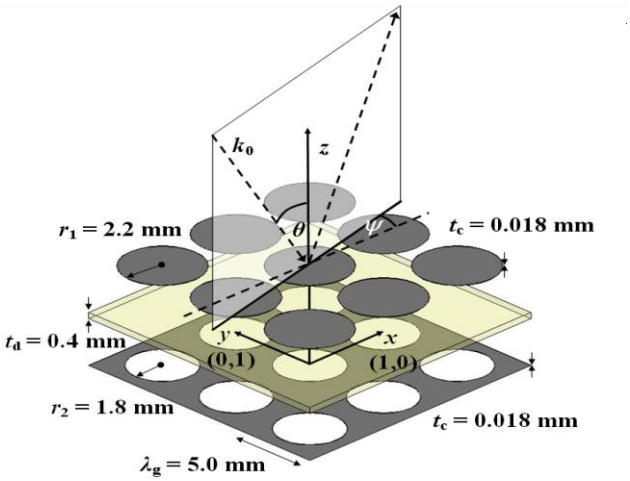

Fig. 1. Schematic of the experimental sample and the coordinate system used. Note that the three layers, patch array (upper), dielectric spacer (middle) and aperture array (lower), have been separated for clarity.

The sample (Fig. 1) is formed by employing conventional printed circuit board (PCB) processing techniques. The PCB substrate is a Nelco® NY9220 material of thickness 0.4 mm and relative permittivity $\varepsilon = 2.2 + 0.002i$ (specified at 10 GHz [19]), coated on each side with 18 μm of copper. Both the patches and apertures reside in a 5 mm pitch square array and have radii of 2.2 mm and 1.8 mm respectively. The total sample area is approximately 350 mm × 350 mm. Transmission spectra for a collimated microwave beam are recorded for incident azimuth angles of $\psi = 0°$, $\psi = 30°$ and $\psi = 45°$ and for incident polar angles $-25° \le \theta \le 25°$, for both transverse magnetic (TM) and transverse electric (TE) polarizations.

Experimental spectral transmission data, normalised to the transmission in the absence of a sample, plotted as a function of frequency and in-plane wavevector for a number of different incident polarizations and sample orientations are shown in Fig. 2.

2. Experimental data and numerical modelling

Figure 3 part (a) illustrates a typical experimental transmission spectrum (TE polarization, $\theta = 10°$ and $\psi = 30°$) together with the predictions from finite element method modelling (FEM) [20]. The predictions of the resonant frequencies using Eq. (1) are also indicated (black vertical dashed lines). Note that the first, second and third order modes are all below the onset of diffraction [52.3 GHz for the lowest diffracted order (± 1,0)]. It is apparent that the predictions from the FEM modelling show good agreement with the experimental data. Note the appearance of a splitting of the second order mode: this phenomenon is discussed in due course.

The prediction from the FEM modelling for the intensity of the third order mode is greater than the experimental data. Further modelling (not shown) indicates that this is associated with the inherent angle spread of the incident beam, exacerbated by the close proximity of this resonance to the (1,0) diffracted light line with which it must interact. It is also apparent that the prediction of the resonant frequencies using [Eq. (1)] is far too simplistic since this expression does not take into account field expansion into the air surrounding the capped aperture array, which acts to shift the resonance up in frequency. FEM modelling shows that the frequency at which the resonance lies will be between the two predictions of Eq. (1) using a refractive index of the Nelco NY9220 and air. Furthermore FEM modelling shows that if the dielectric surrounding the capped aperture array is the same as that between the two FSS then

#132940 - $15.00 USD Received 4 Aug 2010; revised 1 Oct 2010; accepted 3 Oct 2010; published 29 Oct 2010

the predictions of Eq. (1) are accurate, particularly when the layer separation is very small compared to the radial overlap.

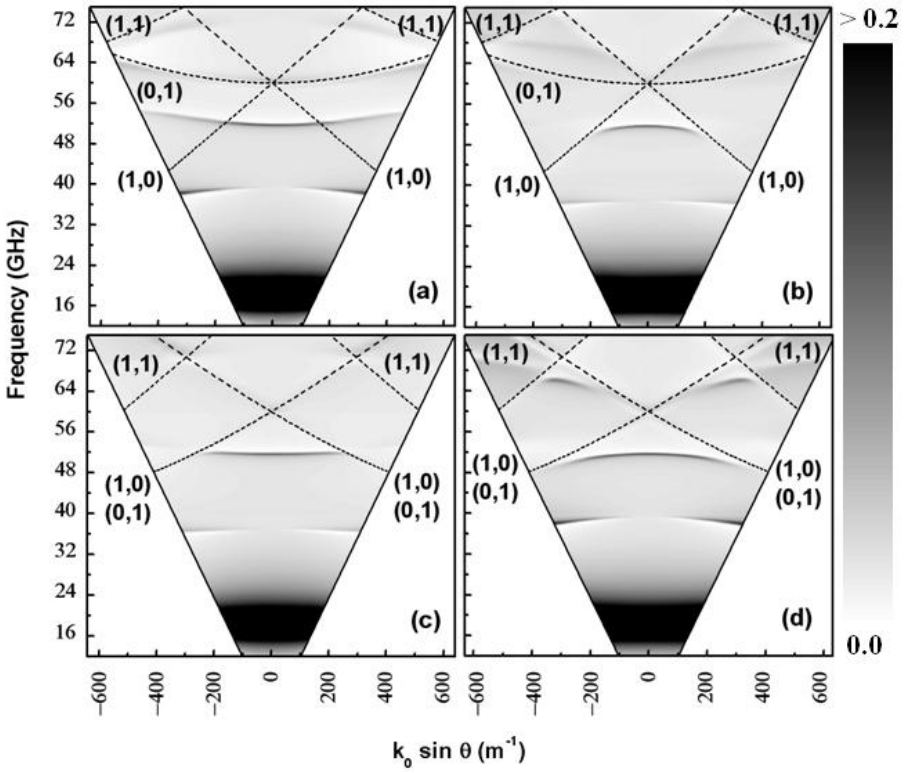

Fig. 2. Experimental spectral transmission as a function of both frequency and in-plane wavevector ($k_{//} = k_0 \sin \theta$) for (a) TE $\psi = 0°$; (b) TM $\psi = 0°$; (c) TE $\psi = 45°$; (d) TM $\psi = 45°$. Diffracted light lines are indicated by black dotted lines, and are labelled with their order (note only magnitude, not direction, is labelled). The transmission intensity is shown on a linear saturated scale from 0.0 (white) to greater than 0.2 (black).

#132940 - $15.00 USD Received 4 Aug 2010; revised 1 Oct 2010; accepted 3 Oct 2010; published 29 Oct 2010

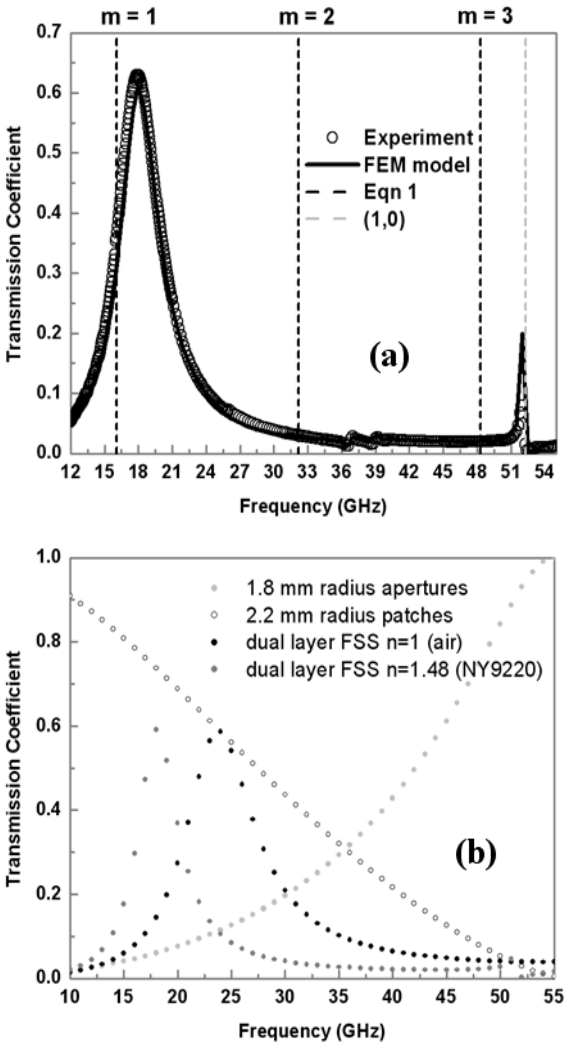

Fig. 3. (a) Experimental data (circles) and FEM modelling (solid thick black line) for TE polarised incident radiation with θ = 10° and ψ = 30°. The dotted black lines represent the predicted resonant frequencies using Eq. (1) of the first, second and third order modes. The dotted grey line shows the (1,0) diffracted light line. (b) FEM predictions of the transmission spectra of the response of the component aperture and patch arrays, together with the dual layer geometry, spaced with air and NY9220 dielectric.

We now employ the FEM model to explore the resonant electromagnetic fields of the structure. Near-field diffraction from the edges of the patch/aperture system couples radiation into the annular cavity bound by the overlapping metal regions. On resonance, the electric fields in the cavity are clearly predominately in the *z*-direction (*i.e.*, normal to the metal surface) and the magnetic fields are primarily in the *xy*-plane [Fig. 4(a) and 4(b)]. The cavity is acting as a high frequency resonant LC-circuit with the resonant modes being quantised azimuthally. The square symmetry of the lattice on which the aperture/patch elements reside permits two different solutions for each allowed quantisation state. In understanding which of the two solutions is excited it is helpful to consider both the incident polarization and azimuth angle.

#132940 - $15.00 USD Received 4 Aug 2010; revised 1 Oct 2010; accepted 3 Oct 2010; published 29 Oct 2010

The first order mode at ~18GHz (Fig. 2), has two antinodes (maxima) in its standing wave fields within the overlap cavity [Fig. 4(c) and 4(f)], the electric and magnetic components are separated both temporally and spatially. If the incident in-plane (*xy*-plane) electric vector (shown by white dotted arrows in Fig. 4) coincides with one of the symmetry planes of the square lattice (i.e. $\psi = 0°$ or $\psi = 45°$) then the electric field maxima must be located along that symmetry plane, and the magnetic field maxima on the orthogonal plane. For all other incident azimuth angles a standing wave solution associated with both of the symmetry planes will be excited. However because these two first order modes are at a frequency far below the diffraction edge they are only weakly perturbed by evanescent diffraction and show no hybridisation. They are therefore degenerate. The first order mode is well below the onset of diffraction (60 GHz at normal incidence) and is non-dispersive to all measured polar angles of incidence, azimuth angles and polarisations. Figures 4(a) and 4(b) shows that the electric fields within the overlap cavity point primarily in the *z* direction whereas the magnetic fields lie primarily in the *xy*-plane. As the overlap is decreased, eventually becoming negative, the resonant frequency drops to a value between those predicted by Eq. (1) using air as a dielectric spacer and NY9220 dielectric as a spacer. As expected as the overlap becomes negative the component of the electric field pointing in the *xy*-plane becomes greater.

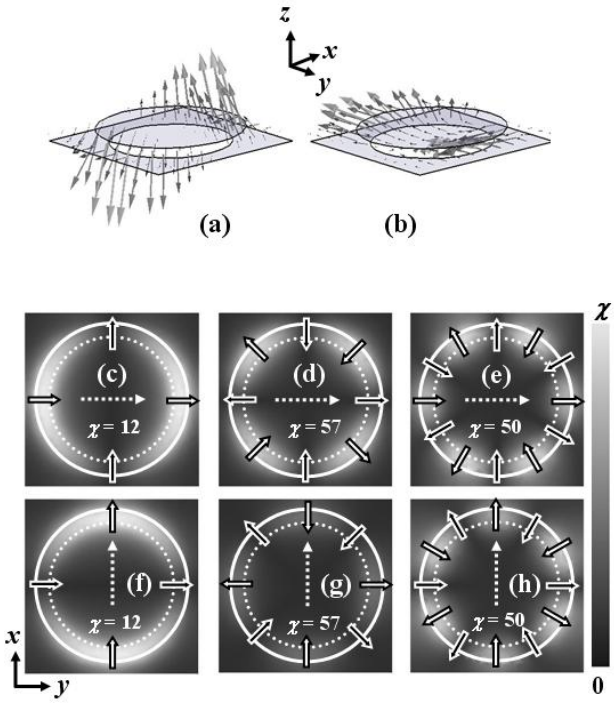

Fig. 4. Field predictions on resonance from the FEM model (a) electric field and (b) magnetic field vectors at a phase corresponding to maximum field enhancement (χ) for the first order mode (TM, $\theta = 5°$, $\psi = 0°$). (c) to (e) illustrate the electric field magnitude on resonance of the first, second and third order modes (c, d and e respectively) for $\theta = 5°$, $\psi = 0°$ and TE polarization. (f) to (h) illustrate the electric field magnitude on resonance of the first, second and third order modes (f, g and h respectively) for $\theta = 5°$, $\psi = 0°$ and TM polarization. Solid black arrows with a white outline and white arrows with a black outline represent the magnetic and electric vector components directions in the *xy*-plane respectively. White dotted arrows depict the in-plane (*xy*-plane) incident electric vectors. Note, (a) to (h) are plotted in the *xy*-plane at an equal distance (0.2 mm) from the patch and aperture array. (c) and (f) show electric field enhancements ranging from 0 to 12, (d) and (g) from 0 to 57, and (e) and (h) from 0 to 50 times the incident field. The solid white line and dotted white line show the outline of the patch and aperture respectively.

#132940 - $15.00 USD Received 4 Aug 2010; revised 1 Oct 2010; accepted 3 Oct 2010; published 29 Oct 2010

The second order mode between ~36 GHz and 40 GHz (Fig. 2), has four antinodes in its standing wave fields within the overlap cavity. Due to symmetry, the in-plane (*xy*-plane) electric field components must point either towards one another or away from one another at opposite side of the patches [Fig. 4(d) and 4(g)]. Thus for normally incident radiation this mode is not excited. A phase delay in the incident radiation as it travels across the patch is required. The electric and magnetic field distribution is the same for TE polarization at $\psi = 0°$ azimuth [Fig. 4(d)] as for TM polarisation at $\psi = 45°$ azimuth, likewise the field distribution for TE radiation at $\psi = 45°$ azimuth is the same as that for TM radiation at $\psi = 0°$ azimuth [Fig. 4(g)]. As this second order mode approaches the (0,1) diffracted light line there is evidence for perturbation by the evanescent diffraction [Fig. 2(a) and 2(d)]. The mode is stronger when the electric fields are spaced further apart between neighbouring elements such as in [Fig. 2(a) and 2(d)] where the high regions of electric field align with the 45° and 135° symmetry planes and weaker in [Fig. 2(b) and 2(c)] where the fields align with the 0° and 90° symmetry planes.

As previously discussed for the first order mode, if the incident in-plane (*xy*-plane) electric vector does not align with one of the symmetry planes of the lattice then the second order mode will have two solutions, one with the same field distribution within the overlap cavity as for the $\psi = 0°$ solution and one the same as the $\psi = 45°$ solution. However the intensities of both modes will differ. This is observed in Fig. 3.

The third order mode at ~51 GHz (Fig. 2), has six antinodes in its standing wave fields within the overlap cavity. Due to its proximity to the diffracted light lines, the modes are highly hybridised forming diffractively coupled surface waves, evident as strong curvature in its dispersion, which follows the light line. For a $\psi = 0°$ azimuth angle, when excited by TE polarized and TM polarized incident radiation the third order mode disperses with the ± (0,1) and ± (1,0) light lines respectively. For a $\psi = 45°$ azimuth angle, when excited by TE polarized and TM polarised incident radiation the third order mode disperses with the degenerate ± (0,1) and ± (1,0) light lines respectively. We note that the TE polarised mode does not appear to interact strongly with the ± (0,1) and ± (1,0) light lines until in very close proximity [Fig. 2(c)]. The electric and magnetic field distribution as noted also for the second order mode, is the same for TE polarisation at $\psi = 0°$ azimuth as for TM polarisation at $\psi = 45°$ azimuth, likewise the field distribution for TE radiation at $\psi = 45°$ azimuth is the same as that for TM radiation at $\psi = 0°$ azimuth [Fig. 4(e) and 4(h)]. There are of course higher order modes, for example the fourth order mode is visible in Fig. 4 at ~65 GHz, above the first order diffracted light lines, but these modes are weakly excited and of little interest. Experimentally we also observe very weak surface modes, manifested just beneath the diffraction edge. Experimentally these modes are less intense than predicted by FEM modelling, due to beam spread and both their narrow width and dispersive nature.

3. Conclusions

The resonant microwave transmission due to an annulus-like resonance in a cavity formed between overlapping metallic surfaces of a capped aperture array has been explored. The dependence on angle of incidence, azimuth angle and polarization has been examined. The first order mode, which is far from the diffraction edge, is broad and largely invariant to changes in incident angle, azimuth angle and polarization. Furthermore the fundamental resonant response of the capped aperture array with air as the dielectric spacer is ~2.3 times lower in frequency than the aperture array alone and with NY9220 dielectric it is ~3.1 times lower. The second order mode which can only be excited at non-normal angles shows a splitting into two distinct modes when the incident in-plane electric vector does not align with one of the symmetry planes of the square lattice. Due to its proximity to the diffracted light lines, the third order mode is influenced by evanescent diffraction, and is strongly dependent on azimuth angle, polarization and angle of incidence. The modes have frequencies dictated primarily by the average radius of the metallic patches and apertures with perturbations

#132940 - $15.00 USD Received 4 Aug 2010; revised 1 Oct 2010; accepted 3 Oct 2010; published 29 Oct 2010

primarily due to field expansion into the surrounding air. This structure could be very useful where high metal content is required for a transmitting frequency selective surface.

Acknowledgements

Funding for this work has been provided through APH's EPSRC Advanced Research Fellowship, and MPB's EPSRC/Dstl Industrial CASE Studentship. The authors would also like thank Melita Taylor and Dr Matthew Lockyear for informative discussions. This work is part funded by the Ministry of Defence and is published with the permission of the Defence Science and Technology Laboratory on behalf of the Controller of HMSO.

#132940 - $15.00 USD Received 4 Aug 2010; revised 1 Oct 2010; accepted 3 Oct 2010; published 29 Oct 2010